# Spatial heterogeneity of cell-matrix adhesive forces predicts human glioblastoma migration

Rasha Rezk, Bill Zong Jia*, Astrid Wendler*, Ivan Dimov, Colin Watts, Athina E Markaki,

Kristian Franze, Alexandre J Kabla

Department of Engineering, University of Cambridge, Trumpington Street, Cambridge CB2 1PZ, UK (RR, BZJ, AEM, AJK). Department of Clinical Neuroscience, University of Cambridge, Cambridge Biomedical Campus, Cambridge, CB2 0QQ (AW, CW). Department of Physiology, Development and Neuroscience, University of Cambridge, Downing Pl, Cambridge CB2 3EL (ID, KF), Birmingham Brain Cancer Program, University of Birmingham, Institute of Cancer and Genomic Sciences, College of Medical and Dental Sciences (CW), Systems, Synthetic, and Quantitative Biology PhD Program, Harvard University, Cambridge, Massachusetts, USA (BZJ)

**Corresponding**

Rasha Rezk

Department of Engineering, University of Cambridge, Trumpington Street, Cambridge CB2 1PZ, UK

Email: rsr33@cam.ac.uk

Telephone: +44 1223 332600

Alexandre Kabla

Department of Engineering, University of Cambridge, Trumpington Street, Cambridge CB2 1PZ, UK

Email: ajk61@eng.cam.ac.uk

*BZJ and AW equal second authors

**Conflict of interest**: The authors report no conflict of interest, and the present study has not been presented elsewhere.

**Authorship**:  R.R. conceptualized and designed the study. RR, BZJ, AW, KF and AJK designed and performed the experiments, derived the models and analyzed the data. ID performed and analyzed the PDMS compound. CW supervised the clinical procedure, provided surgical samples and interpreted clinical data. All authors discussed the data and wrote the manuscript.

**Abstract**

**Background**

Glioblastoma (GBM) is a highly aggressive incurable brain tumor. The main cause of mortality in GBM patients is the invasive rim of cells migrating away from the main tumor mass and invading healthy parts of the brain. Although motion is driven by forces, our current understanding of the physical factors involved in glioma infiltration remains limited. This study aims to investigate the adhesion properties within and between patients' tumors on a cellular level and test whether these properties correlate with cell migration.

**Methods**

Six tissue samples were taken from spatially separated sections during 5-aminolevulinic acid (5-ALA) fluorescence guided surgery. Navigated biopsy samples were collected from strongly fluorescent tumor cores, a weak fluorescent tumor rim, and non-fluorescent tumor margins. A microfluidics device was built to induce controlled shear forces to detach cells from monolayer cultures. Cells were cultured on low modulus polydimethylsiloxane representative of the stiffness of brain tissue. Cell migration and morphology were then obtained using time lapse microscopy.

**Results**

GBM cell populations from different tumor fractions of the same patient exhibited different migratory and adhesive behaviors. These differences were associated with sampling location and amount of 5-ALA fluorescence. Cells derived from weak- and non-fluorescent tumor tissue were smaller, adhered less well, and migrated quicker than cells derived from strongly fluorescent tumor mass.

**Conclusion**

GBM tumors are biomechanically heterogeneous. Selecting multiple populations and broad location sampling are therefore important to consider for drug testing.

3

**Key points**

GBM tumors are biomechanically heterogeneous

GBM cell migration is inversely correlated with cell-matrix adhesion strength

5-ALA fluorescence intensity during surgery correlates with the motility properties of GBM cells

**Importance of the study**

This study shows a clear correlation between the mechanical behaviour of patient derived tumour cells and intraoperative tissue fluorescence using 5-aminolevolinic acid (5-ALA). Using a novel microfluidics approach, we measure cell-matrix adhesive forces (within and between tumor samples) and suggest a biophysical relationship between the characteristics of GBM cells and tumor spatial structure. Cells derived from the weak fluorescent tumor rim, and non-fluorescent tumor margins have different adhesion profiles and are highly migratory compared to those found in the core of the tumor. Not accounting for internal sampling location within each tumor obscures differences in cell morphology, motility and adhesion properties between patients. Preclinical tests aimed at developing a treatment for GBM using anti-invasive drugs or adhesion inhibitors, would benefit from using cell lines derived from the tumor periphery (with low 5-ALA intensity) rather than cell lines derived from the tumor core.

**Introduction**

Glioblastoma (GBM) is the most common and the most malignant brain tumor. No cure is available despite significant improvements in surgical techniques and radiation technology. The extensive and infiltrative growth pattern of GBM makes surgical resection extremely difficult [1] and limits the efficacy of radiation therapy by obscuring tumor margins [2]. Tumor recurrence is inevitable; targeted chemotherapy [3] and immune therapy [4] have failed to stop tumor recurrence.

Migration and invasion are driven by mechanical forces [5]. The mechanical properties of a GBM tumor and its microenvironment have also shown to contribute to tumor invasion [6,7]. GBM employ a mesenchymal mode of migration [8] using focal adhesions proteins as molecular clutches to transmit forces to their environments. Targeting integrins or kinases that mediate cell-matrix adhesion has therefore been explored as a strategy to inhibit tumor growth (e.g. focal adhesion kinase (FAK) inhibitor [9]) or to halt the mesenchymal mode of migration employed by infiltrating GBM cells[10]. However, therapeutics designed to target adhesion receptors or proteases have failed in clinical trials [11], particularly in gliomas (e.g. cilengitide [12]). This failure might be due to the heterogeneity in expression of the adhesion proteins in glioma. Arguably GBM intratumor heterogeneity is the key to understanding treatment failure [13] and infiltration.

GBM tumors show transcriptomic and genomic distinct subclasses [14,15] which vary across patients, but also across individual cells within a tumor [16]. This could explain why gene expression-based molecular classification of brain tumors failed to provide a more accurate prediction of tumor progression and response to treatment. Differential response to treatment is visible during fluorescent guided surgery. GBM cells glow fluorescent pink when 5-aminolevulinic acid (5-ALA) is administered orally prior to surgery. The heterogeneity of 5-ALA-induced PpIX fluorescence observed during surgery was associated with different cellular functions and a distinct mRNA expression profile, where non-fluorescent tumor tissue resembled the neural subtype of GBM and fluorescent tumor tissue did not exhibit a known subtype [17]. However, whether fluorescence heterogeneity is mirrored by physical heterogeneity amongst GBM cells remains unclear.

5

To investigate the different adhesive and migratory properties of GBM subpopulations, we derived tumor cells from different GBM patients, and from different regions within the same tumor. Tissue samples obtained from the same tumor were collected from spatially distinct locations with different 5-ALA fluorescent intensities. We adapted a microfluidic device for detachment of adherent cells through shear stress[18,19]. We demonstrate substantial intra- and inter-tumoral heterogeneity; adhesion strength varied tenfold (from 15 Pa to 150 Pa). Cells from the weak fluorescent tumor rim and non-fluorescent margins were smaller, less adherent with highly migratory behavior, suggesting that differential adhesion and migration speed between subpopulations of cancer cells may contribute to tumor invasion. Such heterogeneity could also explain recently observed differential responses of patients to adhesion-blocking drugs.

**Materials and Methods**

**Sample collection**

Tissue collection protocols complied with the UK Human Tissue Act 2004 (HTA license ref. 12315) and have been approved by the local regional ethics committee (LREC ref. 04/Q0108/60).Tissue samples were derived from newly diagnosed GBM patients who underwent their first surgical resection at Addenbrooke's, Cambridge University Hospitals. Aminolevulinic acid (5-ALA) fluorescence was orally administered four hours before induction of anesthesia at a dosage of 20 mg/kg. Three different regions within the tumor were biopsied. Six tissue samples from two different patients were taken from spatially separated sections using MRI stealth imaging. Navigated biopsy samples were collected from strongly fluorescent tumor cores, a weak fluorescent tumor rim, and non-fluorescent tumor margins (Figure 1A). In addition, three tissue samples from a third patient were collected from similar locations (results described in supplementary material). The patient's clinical information and their molecular biomarker status (IDH mutation and *MGMT* promoter methylation) can be found in Supplementary Table 1.

6

**Derivation of GBM stem-like cells**

Cell derivation and maintenance have previously been described[20]. Briefly, tissue was mechanically minced and enzymatically dissociated before passing through a 40 µm cell strainer. Cells were seeded in serum-free medium (SFM) (phenol red free Neurobasal A) with 2mM l-glutamine and 1% volume/volume (v/v) penicillin/streptomycin (PS) solution with 20 ng/mL human epidermal growth factor, 20 ng/mL zebrafish fibroblast growth factor (FGF-2), 1% v/v B27 SF supplement, and 1% N2 SF supplement. Cells were allowed to form primary aggregates. Spheroid aggregates were collected and plated, onto Engelbreth-Holm-Swarm sarcoma extracellular matrix (ECM, Sigma)–coated flasks (ECM 1:10 dilution with HBSS) and allowed to form a primary monolayer. When the primary monolayer reached 80% confluency, cells were passaged to generate the subsequent monolayers by mechanically and enzymatically dissociating remaining aggregates. Cells were maintained at 37°C and 5% CO2. Experiments were performed using passages 3-9. Cell lines were screened regularly for mycoplasma.

**Immunocytochemistry**

Cells were seeded in duplicates into µ-Dish 35 mm (60,000 cells/ibidi dish). After 48 hours, cells were washed with sterile phosphate buffered saline (PBS, Thermo Fisher) before being fixed in 4% paraformaldehyde for 30 minutes (10 minutes at 4°C followed by 20 minutes at room temperature). Cells were washed and then permeabilized for 4 minutes in 0.2% Triton in PBS. Cells were washed again and incubated in blocking buffer (1% bovine serum albumin (BSA), and 2% normal goat serum (NGS), in PBS) for 1 hour at room temperature before incubating with the primary antibody for 2 hours. The following primary antibodies were used: Nestin (Abcam, ab22035, 1:100), Vimentin (Abcam, ab8069, 1:200), NG2 (Abcam, ab83178, 1:200), Ki67 (Abcam, ab16667, 1:200), Vinculin (FAK100, Sigma 1:200), F-actin (FAK100, Sigma 1:500). Secondary antibodies were applied for 1 hour (goat anti-mouse Alexa Fluor 488 pre-adsorbed abcam, 1:750 dilution and goat anti-rabbit Alex Fluor 594 pre-adsorbed abcam, 1:750). Nuclei were stained with DAPI (Roche)

**Immunoblotting**

Cell lysis was performed using cOmpleteTM, EDTA-free lysis-M buffer with protease inhibitor (Roche). Protein concentrations were determined using PierceTM BCA kit (Thermo ScientififTM). Equivalent amounts of protein were electrophoresed on SDS-polyacrylamide gels. The gels were then electroblotted onto PVDF membranes. After blocking with Odyssey Blocking Buffer (TBS) (LI-COR), membranes where incubated with the primary antibody overnight (Paxilin, Vinculin, FAK, GAPDH (codes need to be looked up at home). Finally, the relevant protein was visualized by staining with the appropriate IgG H&L secondary antibody coupled to either IRDye® 800CW or IRDye® 680RD. The antigen of interest was detected using the LI-COR Odyssey CLx Infrared Imaging System. Results were analysed using ImageStudio.

**Poly-di-methyl-siloxane (PDMS) substrates for studying cellular motility and morphology**

NuSil GEL-8100 (NuSil) was prepared in a 1:1 ratio of component A and component B and mixed well for 60 seconds. 1% (w/w) 10:1 (base/crosslinker w/w) Sylgard-184 (VWR) was added to the GEL-8100 and mixed well for 60 seconds. For cell morphology experiments approximately 120mg of the PDMS was added to μ-Dish 35 mm (120mg/dish). For cell migration experiments 80mg/well of PDMS was added to 24-well culture plates (Corning Life Science, Tewksbury, MA, USA). Coated vessels were baked at 65∘C for 13 hours. This treatment gave a shear modulus value of G =1.53±0.12 kPa, n = 16, verified by atomic force microscopy (AFM) indentation. The AFM setup consisted of a JPK CellHesion 200 scanner, and the indentation probe was made by gluing a spherical polystyrene particle (90 um diameter), to a tipless AFM probe (SHOCON-TL, k ~ 0.1 N/m). Vessels were sterilized by immersion in 70% (v/v) ethanol in distilled water for 15 minutes, followed by two rinses with PBS. The PDMS surface was coated with ECM at a concentration corresponding to a surface density of 6.67 μg/ml assuming complete adsorption.

8

**Cell detachment assay**

Microfluidic devices were manufactured (Supplementary information S1) and sterilized by immersing in 70% ethanol in distilled water (v/v) in a Petri dish, and perfusing with the same liquid at 10 mL/h for 30 minutes. The devices were lifted from the ethanol and perfused with phosphate-buffered saline (PBS, Thermo-Fisher) at 5 mL/h for 1 hour to rinse the ethanol and allow PBS to permeate the bulk of the device. The devices were filled with 200 μg/mL ECM matrix and placed in the incubator overnight (approximately 16 hours). SFM was equilibrated overnight in the incubator to minimize bubble formation. Cells were detached as described previously and resuspended to a concentration of $3.5 \times 10^{\wedge}6$ cells/mL. Cells were loaded into 1mL syringes and perfused into the devices at 30 μL/h for 5 minutes. Perfusion was resumed for 3 minutes with the inlet and outlet reversed to seed cells evenly. The devices were placed in the incubator for 4 hours to promote cell attachment. The devices were then perfused for 20 hours with equilibrated SFM at a flow rate of 10 μL/h to allow cells to fully spread [21-23]. For cell detachment, neurobasal Medium without supplements was also equilibrated overnight in the incubator to minimize bubble formation and to control dissolved gas concentration and pH. Cells were subjected to a steady flow rate of 0.16 mL/min, 0.33 mL/min and 0.5 mL/min to create a constant shear force on the cell (Supplementary information S1).Phase-contrast images of a single field of view were taken every two seconds at 160×magnification (Zeiss Axio Observer.Z1). The maximum flow rate used was 0.5 mL/min, (a shear stress of 75.96 Pa), although shear stress of up to 506 Pa is achievable with the system, limited by the maximum flow rate of the syringe pump.

**Time lapse measurements and cell tracking analysis**

Cells were cultured in 24-well culture plates (Corning Life Science, Tewksbury, MA, USA) according to the manufacturer's instructions and visualized using a real-time cell imaging system (IncuCyte™ live-cell ESSEN BioScience Inc, Ann Arbor, Michigan, USA). Ten thousand cells/well were cultured on PDMS substrate of 1.5 kPa stiffness. Cells were seeded in triplicates and imaged every 10 min for 48 hours. Time-lapse images were acquired with IncuCyte, a live cell imaging microscope.

Raw images were processed in CellProfiler[24] to detect cell outlines. Cells were tracked using automated tracking in TrackMate[25]. Cell area was calculated after 24 hours , using the hierarchical K-means thresholding module in Icy[26]. The mean square displacement (MSD) of each cell from its starting position

9

was calculated. The MSD of actively moving cells should be larger than the expected MSD of a freely diffusing (Brownian) particle of comparable size:

$$MSD > \frac{K_B T}{3 \pi \eta r} t$$

where $K_B$ is the Boltzmann constant, $T = 310$ K the absolute temperature, $\eta$ the viscosity of the medium, $r$ the radius of the cell and $t$ the time interval. We assumed the viscosity of the medium to be $\eta \approx 0.78$ mPa s.

## Statistical analysis

Data were verified from at least two independent biological experiments. For experiments involving single-cell analysis, n ≥ 100 cells. The order of data collection was randomized; no blinding was performed and no data were excluded from the analysis.

Morphological differences between patients and fluorescence groups were tested using linear regression. First, we tested differences between patients and differences between fluorescence groups independently. Then we tested for differences simultaneously using an additive model (for patients and fluorescence intensity). Since there was no statistically significant difference between weak- and non-fluorescent cell lines but both were different from strongly fluorescent cell lines, we pooled the weak- and non-fluorescent groups. To check whether sampling from multiple locations violated our standard linear model assumptions, we tested unexplained heterogeneity using mixed effect regression. Including a random effect of all lines did not significantly improve model fit. This indicates that a mixed effect model is not required.

Adhesion heterogeneity between cell lines was analyzed using Welch's *t*-test (unequal variance) with Bonferroni correction (15 comparisons). The shear stress required for 50% cell detachment was found by performing an orthogonal distance regression, and the resulting fitted values and associated standard errors were used in the Welch's *t*-test formula. Differences in cell migration between patients and fluorescence groups were tested using weighted linear regression (using MSD slope estimate as the outcome). First, we tested differences between patients and differences between fluorescence groups independently. After pooling the weak- and non-fluorescent cell lines, we tested for differences simultaneously using an additive model (for patients and fluorescence intensity).

10

Statistical analyses and plotting were performed in Python 3.6, MATLAB or R statistical software package.

## Results

### Relationship between tissue fluorescence heterogeneity and GBM cell morphology

Primary GBM cell lines maintained in serum-free media expressed neural stem cell markers nestin and vimentin (Figure 1B). This confirmed the presence of glioma stem-like cells which are regarded as tumorigenic and associated with the heterogeneity in GBM [27] . We then investigated the cell spreading area which is known to be an indicator of how cells mechanically interact with their extracellular environment[28].

Cells were cultured on polydimethylsiloxane, with a low modulus consistent with the stiffness of the environment that GBM infiltrate, which ranges from 0.1 kPa to 10 kPa [29] . Glioma cells are known to spread on substrates of stiffness around 1kPa[30]However, on extremely compliant substrate (~150 Pa) GBM cells exhibit rounded morphologies with diffuse distributions of F-actin that are unable to migrate productively[31]. To compare between lines, we used a single stiffness, ~1.5kPa (Methods) (Figure 1C).

To explain the variability in cell morphology observed among patients' cell lines (Figure ID), we first tested whether cells from patient A differed from those of patient B. Cells derived from patient A exhibited a more elongated morphology compared to cells derived from patient B (***p < 0.001), but there was no significant difference in cell area (p=0.1). However, cells derived from strongly fluorescent lines differed significantly in cell area and cell elongation between patients (***p < 0.001). We therefore adjusted our model to account for fluorescence intensity when comparing between patients (Methods). We found that cells from patient A were both larger and more elongated than cells derived from patient B (***p<0.001).

The results demonstrate morphological differences within each tumor and between tumors and show that this heterogeneity is related to 5-ALA fluorescence intensity. Not accounting for this variability obscured the difference between patients. To investigate whether the differences in cell morphology relate to the

11

way cells adhere to their environment, we explored whether heterogeneity in cell area and shape correlate with specific patterns of key cytoskeletal proteins.

## The organisation of actin filaments and vinculin suggests intertumoral heterogeneity in GBM cell-matrix adhesion

Actin filament disassembly is required for cell spreading, and the binding to proteins such as paxillin and vinculin is necessary for focal adhesion development [32]. We imaged the localization and structure of actin filaments and the actin binding protein vinculin. The shape and distribution of actin and vinculin differed between cells derived from strongly fluorescent lines and cells derived from weak- and non-fluorescent lines. The colocalization of vinculin with F-actin was evident at the edge of cells derived from strongly fluorescent lines (Figure 2A). Adhesion proteins paxillin, vinculin and Focal Adhesion Kinase (FAK) were expressed across all cell lines (Supplementary Figure S1), but their expression levels did not reflect the arrangements and assemblies revealed in immunocytochemical images. The binding of vinculin to F-actin suggests spatial differences in focal adhesion assembly and enlargement within the tumor. We therefore built a set-up to quantify the intra-and-inter tumoral heterogeneity in cell-matrix adhesion.

## Cell-matrix adhesion heterogeneity within and between patient-specific tumor samples

To quantify adhesion strength within GBM cell population, we built a microfluidic device that supported overnight culture of GBM cells and generated sufficient shear force to trigger cells detachment (Supplementary Figure S2). Patients' derived cells were delivered into the channels via syringe pumps ($3.5 \times 10^6$cells /mL). Cells were gently perfused with serum free medium and placed in an incubator for 24 hours to allow adhesion to fully establish and cells to fully spread [21-23]. Cells were subjected to a controlled flow rate to create a constant shear force on the cell (Supplementary information S1). The fraction of detached cells was measured over time (Figure 3A). We consistently found an initial phase of rapid detachment followed by a second phase of slower detachment (Figure 3B), consistent with previous parallel-plate and microfluidic detachment assays [33,34]. This transition manifests itself in most experiments as a "knee" in the time-detachment curve after the first 5 to 10 minutes of exposure to the shear force (Supplementary Figure S3).

12

There is some evidence suggesting that the second phase is a result of adhesion weakening in response to imposed flow, driven by Rho regulation of focal contact maturation and turnover [35,36]. As a consequence, cell detachment measurements taken later in time may not be representative of cell-matrix adhesion under normal condition. We chose to take measurements of detachment at 5 minutes of flow, as a quantification of adhesion strength (Supplementary Figure S3).

Detachment at 5 minutes was expressed as a fraction of the cell number at t=0. Detachment fraction as a function shear stress was fitted to a logistic function, and the shear stress required for 50% detachment ($\tau_d$) was identified. as the inflection point of the logistic fit (Figure 3C). $\tau_d$ ranged between 15 Pa and 141 Pa. This range is consistent with microfluidic single-cell adhesion strength measurements of 3T3 fibroblasts, which fell between 20 and 220 Pa[19].

Cells derived from weak- and non-fluorescent cell lines had significantly lower cell-matrix adhesion than cells derived from strongly fluorescent cell lines across patients A and B (*p < 0.05) (Figure 3D), and smaller cell spreading area (Figure 3E). The mean value of detachment strength of patient B was significantly higher than that of patient A (**p = 0.005). The data shows that both intra- and inter-tumoral cell-matrix adhesion heterogeneity is present within GBM.


**Migratory behavior of tumor derived cell populations is predicted by adhesive forces**

To measure the migratory behavior of GBM cells, we recorded their trajectory on a compliant PDMS substrate. Their movement is stochastic at the scale of 10 mins and is best characterized by an effective diffusion coefficient D which capture the rate of change of the squared end-to-end distance travelled (Mean square displacement (MSD) $\Delta R^2$) as a function of time interval $\Delta T$: $\Delta R^2 = D\ \Delta T$. The larger D, the more migratory the cell line is.

We tested for differences in diffusion coefficient D using an additive model (to account for patients and fluorescence intensities), see Methods, and found that cells from patient B migrated faster than patient A (*p<0.05). Cells derived from strongly fluorescent tissue samples were significantly slower than cells derived from weak- and non-fluorescent cell lines (**p < 0.01) (Figures 4A), had a larger area (Figure 4B) and higher adhesion strength (Figure 4C). This result is consistent with previous models of pseudopodial

13

migration, in which a certain level of adhesion is required for generation of traction forces, but excessive

adhesion impedes motion [37]. Additionally this observation suggested a potential mechanism for differential

diffusion.

**Discussion**

In order to invade the surrounding tissue, GBM cells have to exert forces on their environment and

mechanically interact with it. They also have to undergo biological and morphological changes that allow

them to migrate through the perivascular spaces and white matter tracts of the brain [10]. Instead of

observing the tumor tissue *in* vivo, our approach isolated cell lines (from different tumor regions with

different intraoperative 5-ALA-induced fluorescence intensities) and measured their adhesive and

migratory properties under controlled conditions allowing direct comparison. The results are therefore not

confounded by any spatial differences in extracellular matrix composition, nutrient and oxygen

availability.

. Our findings establish that patient-derived tumor cells have distinct adhesion profiles, that were

reproducible and consistent over several passages (Figure 3B). These profiles were strongly associated

with different migration behaviours, cell size (rather than shape Supplementary Figure S4), tissue sampling

locations and strong vs weak 5-ALA fluorescence. The relationship was further confirmed by analysing a

third patient whose tissue samples were obtained from three similar locations in the tumour; the derived

cell lines exhibited similar morphology (Supplementary Figure S5), adhesive (Supplementary Figure S6)

and migratory behaviour (Supplementary Figure S7). The migratory and adhesion properties of the cell

lines were stable over several passages (Figure 4A, 3B, Supplementary Figure 6A, 7A) for the same

microenvironment. This suggests that the observed biomechanical heterogeneity reflects specific cell

populations rather than cellular plasticity as seen for the expression of various cell surface markers

commonly used to define stem cell populations [27,38]. However, in order to validate this hypothesis, both cell

lines and original tumour samples should be genetically tested and analysed for differences in their

mutational and copy number landscape.

14

The fact that adhesion strength is associated with reduced movement[39] in vitro suggests a simple model where migratory forces must overcome adhesion forces to generate motion. This idea was tested numerically (Supplementary information S2) in order to relate MSD curves with the measured values of cell adhesion. This approach can be extended to simulate mixed populations of core and marginal cells. The variation in adhesion strength leads to variations in amount of migration, causing cells with lower adhesion to be predominant at the leading edge, consistent with the clinical observation (Supplementary Figure S8). This suggests that differential migration may play a role in the spatial distribution of cells within tumor. Differential migration is known to contribute to cell segregation[40]. GBM intratumoral cell proliferation is strongly associated with the fluorescence intensity of samples, and hence the spatial density and distribution of cells.

Recently it has also been shown that fluorescent and non-fluorescent tissue samples can be distinguished genetically [17]. Due to our controlled experimental conditions, much of the observed intra- and inter-tumoral heterogeneity is likely to be of genetic or epigenetic origin, rather than caused by spatial differences in the original tissue's microenvironment. A relationship between glioma mechanics, genetic profiles and epithelial-mesenchymal transition marker expression) and intraoperative techniques (e.g. 5ALA intensities, stealth imaging), would provide a greater understanding of why specific tumour subtypes are more or less sensitive to current therapeutics.

Our results are consistent with a broader picture of GBM as a genetically heterogeneous cancer [13,16]. The human genome encodes 24 different integrin subunits[41], which are highly heterogeneously expressed within GBM[42-44]. These integrins have varying degrees of cross-specificity in both the natural ECM ligands and synthetic inhibitor molecules they can bind. Our results and previous experimental [45] and theoretical work[37] support the hypothesis that the migratory phenotype is linked with cell adhesive forces. Inhibition of one or a few integrins may not significantly change cell-adhesive forces, due to the aforementioned redundancy or compensation through feedback loops that may themselves be driven by cellular mechanosensing[46]. Integrin inhibitors for glioma therapy have been assessed primarily by their affinity and specificity for the target molecule and their ability to arrest tumour growth[47]. Our approach of

15

directly measuring adhesive provides an overall quantitative assessment the strength of cell adhesion that accounts for the presence of integrins and enables a direct correlation with migration data.

Patients' differential response to adhesion inhibitors and anti-invasive molecular treatments maybe due to intrinsic differences in GBM cell motility, adhesion and traction forces. Preclinical tests of adhesion-block typically  use only one or two tumor core cell lines, which may not be representative of the distribution of integrin expression and adhesion in GBM tumors. Given that integrins play a crucial role in brain tumor infiltration [48] and GBM intratumor variability in integrin expressions [49]. New trials that aim to halt GBM recurrence by inhibiting radiation-induced invasion gains and signaling changes [10,50], or kinase inhibitors[9], could benefit from accounting for intra-and-intertumoral differences in cell migration.

# References

1.    Westphal M, Lamszus K. The neurobiology of gliomas: from cell biology to the development of therapeutic approaches. *Nature Reviews Neuroscience.* 2011; 12(9):495.

2.    Price S, Jena R, Burnet N, et al. Improved delineation of glioma margins and regions of infiltration with the use of diffusion tensor imaging: an image-guided biopsy study. *American journal of neuroradiology.* 2006; 27(9):1969-1974.

3.    Sage W, Guilfoyle M, Luney C, et al. Local alkylating chemotherapy applied immediately after 5-ALA guided resection of glioblastoma does not provide additional benefit. *Journal of Neuro-Oncology.* 2018; 136(2):273-280.

4.    Schalper KA, Rodriguez-Ruiz ME, Diez-Valle R, et al. Neoadjuvant nivolumab modifies the tumor immune microenvironment in resectable glioblastoma. *Nature Medicine.* 2019; 25(3):470-476.

5.    Hall A. The cytoskeleton and cancer. *Cancer and Metastasis Reviews.* 2009; 28(1):5-14.

6.    Grundy TJ, De Leon E, Griffin KR, et al. Differential response of patient-derived primary glioblastoma cells to environmental stiffness. *Scientific Reports.* 2016; 6:23353.

7.    Ulrich TA, de Juan Pardo EM, Kumar S. The mechanical rigidity of the extracellular matrix regulates the structure, motility, and proliferation of glioma cells. *Cancer research.* 2009; 69(10):4167-4174.

8.    Paulus W, Baur I, Beutler AS, Reeves SA. Diffuse brain invasion of glioma cells requires beta 1 integrins. *Laboratory investigation; a journal of technical methods and pathology.* 1996; 75(6):819-826.

9.    Brown NF, Williams M, Arkenau H-T, et al. A study of the focal adhesion kinase inhibitor GSK2256098 in patients with recurrent glioblastoma with evaluation of tumor penetration of [11C] GSK2256098. *Neuro-oncology.* 2018; 20(12):1634-1642.

10.   Birch JL, Strathdee K, Gilmour L, et al. A novel small-molecule inhibitor of MRCK prevents radiation-driven invasion in glioblastoma. *Cancer research.* 2018; 78(22):6509-6522.

11.   Friedl P, Wolf K. Tumour-cell invasion and migration: diversity and escape mechanisms. *Nature Reviews Cancer.* 2003; 3(5):362-374.

12.   Stupp R, Hegi ME, Gorlia T, et al. Cilengitide combined with standard treatment for patients with newly diagnosed glioblastoma with methylated MGMT promoter (CENTRIC EORTC 26071-22072 study): a multicentre, randomised, open-label, phase 3 trial. *The lancet oncology.* 2014; 15(10):1100-1108.

13.   Sottoriva A, Spiteri I, Piccirillo SGM, et al. Intratumor heterogeneity in human glioblastoma reflects cancer evolutionary dynamics. *Proceedings of the National Academy of Sciences of the United States of America.* 2013; 110:4009-4014.

14.   Verhaak RG, Hoadley KA, Purdom E, et al. Integrated genomic analysis identifies clinically relevant subtypes of glioblastoma characterized by abnormalities in PDGFRA, IDH1, EGFR, and NF1. *Cancer cell.* 2010; 17(1):98-110.

15.   Brennan CW, Verhaak RG, McKenna A, et al. The somatic genomic landscape of glioblastoma. *Cell.* 2013; 155(2):462-477.

16.   Patel AP, Tirosh I, Trombetta JJ, et al. Single-cell RNA-seq highlights intratumoral heterogeneity in primary glioblastoma. *Science (New York, N.Y.).* 2014; 344:1396-1401.

17.   Damian AAB, Matthew CH, Myung Chang L, et al. Characterizing the heterogeneity in 5-aminolevulinic acid–induced fluorescence in glioblastoma. *Journal of Neurosurgery JNS.* 2019:1-9.

18.   Lu H, Koo LY, Wang WM, Lauffenburger DA, Griffith LG, Jensen KF. Microfluidic shear devices for quantitative analysis of cell adhesion. *Analytical Chemistry.* 2004; 76:5257-5264.

19.   Christ KV, Williamson KB, Masters KS, Turner KT. Measurement of single-cell adhesion strength using a microfluidic assay. *Biomedical Microdevices.* 2010; 12:443-455.

**20.** Fael Al-Mayhani TM, Ball SLR, Zhao J-W, et al. An efficient method for derivation and propagation of glioblastoma cell lines that conserves the molecular profile of their original tumours. *Journal of Neuroscience Methods.* 2009; 176(2):192-199.

**21.** Kim Y, Kumar S. CD44-mediated adhesion to hyaluronic acid contributes to mechanosensing and invasive motility. *Molecular Cancer Research.* 2014; 12(10):1416-1429.

**22.** Cuvelier D, Théry M, Chu Y-S, et al. The universal dynamics of cell spreading. *Current biology.* 2007; 17(8):694-699.

**23.** Huang W, Anvari B, Torres JH, LeBaron RG, Athanasiou KA. Temporal effects of cell adhesion on mechanical characteristics of the single chondrocyte. *Journal of orthopaedic research.* 2003; 21(1):88-95.

**24.** Kamentsky L, Jones TR, Fraser A, et al. Improved structure, function and compatibility for CellProfiler: modular high-throughput image analysis software. *Bioinformatics.* 2011; 27(8):1179-1180.

**25.** Tinevez J-Y, Perry N, Schindelin J, et al. TrackMate: An open and extensible platform for single-particle tracking. *Methods.* 2017; 115:80-90.

**26.** De Chaumont F, Dallongeville S, Chenouard N, et al. Icy: an open bioimage informatics platform for extended reproducible research. *Nature methods.* 2012; 9(7):690.

**27.** Dirkse A, Golebiewska A, Buder T, et al. Stem cell-associated heterogeneity in Glioblastoma results from intrinsic tumor plasticity shaped by the microenvironment. *Nature communications.* 2019; 10(1):1787.

**28.** Vining KH, Mooney DJ. Mechanical forces direct stem cell behaviour in development and regeneration. *Nat Rev Mol Cell Biol.* 2017; 18(12):728-742.

**29.** Koser DE, Thompson AJ, Foster SK, et al. Mechanosensing is critical for axon growth in the developing brain. *Nature neuroscience.* 2016; 19(12):1592.

**30.** Pogoda K, Bucki R, Byfield FJ, et al. Soft substrates containing hyaluronan mimic the effects of increased stiffness on morphology, motility, and proliferation of glioma cells. *Biomacromolecules.* 2017; 18(10):3040-3051.

**31.** Sen S, Kumar S. Cell–matrix de-adhesion dynamics reflect contractile mechanics. *Cellular and molecular bioengineering.* 2009; 2(2):218-230.

**32.** Maziveyi M, Alahari SK. Cell matrix adhesions in cancer: the proteins that form the glue. *Oncotarget.* 2017; 8(29):48471.

**33.** Truskey GA, Pirone JS. The effect of fluid shear stress upon cell adhesion to fibronectin-treated surfaces. *Journal of Biomedical Materials Research.* 1990; 24:1333-1353.

**34.** van Kooten TG, Schakenraad JM, Van der Mei HC, Busscher HJ. Development and use of a parallel-plate flow chamber for studying cellular adhesion to solid surfaces. *Journal of Biomedical Materials Research.* 1992; 26:725-738.

**35.** Civelekoglu-Scholey G, Wayne Orr A, Novak I, Meister J-J, Schwartz MA, Mogilner A. Model of coupled transient changes of Rac, Rho, adhesions and stress fibers alignment in endothelial cells responding to shear stress. *Journal of Theoretical Biology.* 2005; 232:569-585.

**36.** Tzima E, del Pozo MA, Shattil SJ, Chien S, Schwartz MA. Activation of integrins in endothelial cells by fluid shear stress mediates Rho-dependent cytoskeletal alignment. *The EMBO Journal.* 2001; 20:4639-4647.

**37.** DiMilla P, Barbee K, Lauffenburger D. Mathematical model for the effects of adhesion and mechanics on cell migration speed. *Biophysical journal.* 1991; 60(1):15-37.

**38.** Al-Mayhani TF, Heywood RM, Vemireddy V, Lathia JD, Piccirillo SG, Watts C. A non-hierarchical organization of tumorigenic NG2 cells in glioblastoma promoted by EGFR. *Neuro-oncology.* 2019; 21(6):719-729.

**39.** Montell DJ. Morphogenetic cell movements: diversity from modular mechanical properties. *Science.* 2008; 322(5907):1502-1505.

40. Siegert F, Weijer CJ. Three-dimensional scroll waves organize Dictyostelium slugs. *Proceedings of the National Academy of Sciences.* 1992; 89(14):6433-6437.
41. Takada Y, Ye X, Simon S. The integrins. *Genome biology.* 2007; 8(5):215.
42. Yuan B-Z, Miller MJ, Keck CL, Zimonjic DB, Thorgeirsson SS, Popescu NC. Cloning, characterization, and chromosomal localization of a gene frequently deleted in human liver cancer (DLC-1) homologous to rat RhoGAP. *Cancer research.* 1998; 58(10):2196-2199.
43. Riemenschneider MJ, Betensky RA, Pasedag SM, Louis DN. AKT activation in human glioblastomas enhances proliferation via TSC2 and S6 kinase signaling. *Cancer research.* 2006; 66(11):5618-5623.
44. Weller M, Van den Bent M, Hopkins K, et al. European Association for Neuro-Oncology (EANO) Task Force on Malignant Glioma. EANO guideline for the diagnosis and treatment of anaplastic gliomas and glioblastoma. *Lancet Oncol.* 2014; 15(9):e395-e403.
45. Zaman MH, Trapani LM, Sieminski AL, et al. Migration of tumor cells in 3D matrices is governed by matrix stiffness along with cell-matrix adhesion and proteolysis. *Proceedings of the National Academy of Sciences.* 2006; 103(29):10889-10894.
46. Gardel ML, Schneider IC, Aratyn-Schaus Y, Waterman CM. Mechanical integration of actin and adhesion dynamics in cell migration. *Annual review of cell and developmental biology.* 2010; 26:315-333.
47. Oliveira-Ferrer L, Hauschild J, Fiedler W, et al. Cilengitide induces cellular detachment and apoptosis in endothelial and glioma cells mediated by inhibition of FAK/src/AKT pathway. *Journal of Experimental & Clinical Cancer Research.* 2008; 27(1):86.
48. Friedlander DR, Zagzag D, Shiff B, et al. Migration of brain tumor cells on extracellular matrix proteins in vitro correlates with tumor type and grade and involves $\alpha v$ and $\beta 1$ integrins. *Cancer research.* 1996; 56(8):1939-1947.
49. Malric L, Monferran S, Gilhodes J, et al. Interest of integrins targeting in glioblastoma according to tumor heterogeneity and cancer stem cell paradigm: an update. *Oncotarget.* 2017; 8(49):86947.
50. Kegelman TP, Wu B, Das SK, et al. Inhibition of radiation-induced glioblastoma invasion by genetic and pharmacological targeting of MDA-9/Syntenin. *Proceedings of the National Academy of Sciences.* 2017; 114(2):370-375.

**Figure 1: Fluorescence and Morphological Characteristics of GBM Patients Derived Cell Line**s

(A) White light image of resection cavity and corresponding fluorescence view of surgical field demonstrating the heterogeneous fluorescence pattern of 5-ALA (bright strong pink from tumor core, faint/weak pink from tumor rim, and non-fluorescent tumor margin). Intraoperative images were obtained via ZEISS OPMI PENTERO 800, with 39x magnification. We collected three strongly fluorescent tissue samples from the tumor mass (S from patient A, S1 and S2 from patient B), two non-fluorescent tumor margins (N1 and N2) from patient A, and one weak-fluorescent tissue sample (W) from patient B.

(B) Immunofluorescence staining for evidence of GBM stem like cells. Neural stem cell marker nestin (green), and vimentin (green) are expressed in each cell line; scale bars 20 μm.

(C) Representative phase-contrast images showing cells derived from strong fluorescent tissue samples has larger area compared to cells derived from weak- and non-fluorescent samples. Patient A exhibited a more elongated morphology compared to patient B (***p<0,.001); scale bars 100 μm. At least three independent experiments were carried out, with at least 360 cells analyzed per patient. Or/ Between 360 - 500 cells were analysed from at least three independent experiments per patient.

(D) Morphological quantification of cells cultured on PDMS substrates of ~1.5kPa stiffness. Boxplots show spatial and intertumoral heterogeneity in cell area and cell elongation. Boxplots represent the "minimum", first quartile (Q1), median, third quartile (Q3), and maximum. At least 110 (or Between 110-180 cells) cells were analysed from at least two independent experiments.

**Figure 2. F-actin cytoskeleton and Vinculin proteins expression in GBM lines**

Confocal images showing the colocalization of vinculin and F-actin at the edge of cells derived from strong fluorescent lines compared to cells derived from weak- and non-fluorescent lines. Cells were stained with TRITC-phalloidin (red) to visualize the actin cytoskeleton, vinculin (green) and DAPI (blue). Scale bars 40 μm.

**Figure 3: GBM exhibits spatial and inter-tumor heterogeneity in cell-matrix adhesion.**

(A) Representative phase-contrast images of cells under microfluidic shear detachment at 0, 150, and 300 seconds. Here BW cells are exposed to 0.33 mL/min of flow, corresponding to 51 Pa of shear stress. Scale bars 100 μm.

(B) For each condition (shear flow), detachment-time curve were generated using two independent experiments per cell line (25-138 cells per experiment).Detachment increases with shear stress, but the relative ordering of the lines remains constant except for cell line AS. Detachment initially occurs rapidly, and plateaus for most cell lines.

(C) The inflection point of each sigmoidal curve was extracted to define $\tau_d$, a measurement for the cell-matrix adhesion strength of the cell lines.

(D) Differences between weak- and strongly-fluorescent lines were statistically significant for all intra-patient pairs except BW and BS2 (one * indicates (*p <0.05) and additional *s indicates further orders of magnitude, under Welch's t-test with Bonferroni correction). The mean value of $\tau_d$ for patient B was significantly higher than that of patient B (**p = 0.005).

(E) Relationship between cell spread area and cell-matrix adhesion strength. Strong fluorescent cells are more adherent and larger than weak- and non-fluorescent cells. Error bars represent SEM from at least two independent experiments.

**Figure 4. Cell-matrix adhesion is an important factor for GBM cell migration**

(A) MSD as a function of time interval (Δt) calculated from cell trajectories with vertical bars representing standard errors. At least 100 cells were analysed from two independent experiments.. Having accounted for tissue fluorescence intensity, we found that cells from patient B migrated faster than patient A (*$p<0.05$). Cells derived from strongly fluorescent tissue samples were significantly slower than cells derived from weak- and non-fluorescent cell lines (**$p < 0.01$).

(B) Cells with larger cell area migrate less than those with smaller cell size derived from the weak- and non-fluorescent samples. Error bars represent SEM from at least two independent experiments.

(C) Cells derived from strong fluorescent tissue samples are more adhesive and less migratory. Error bars represent SEM from at least two independent experiments.
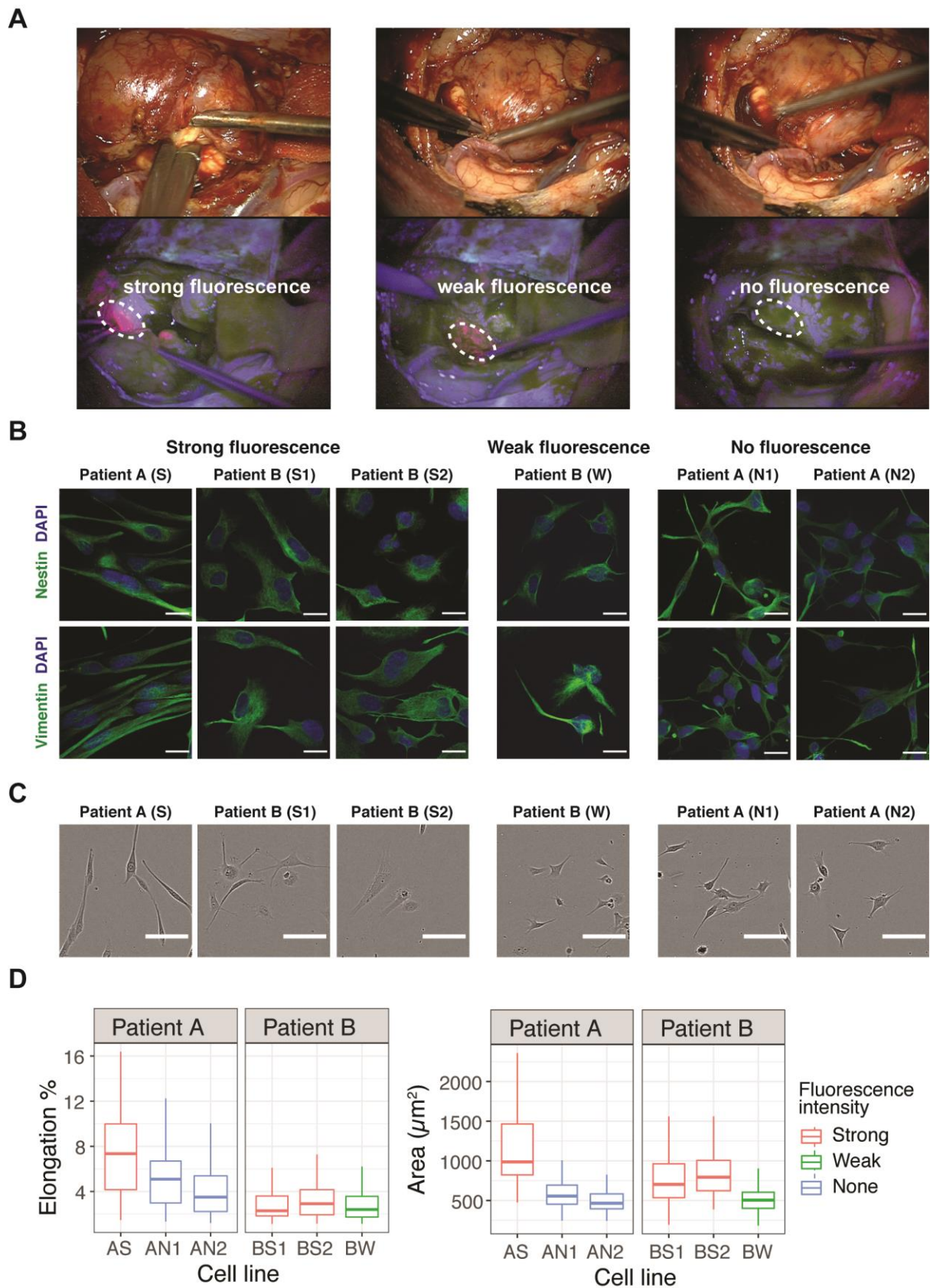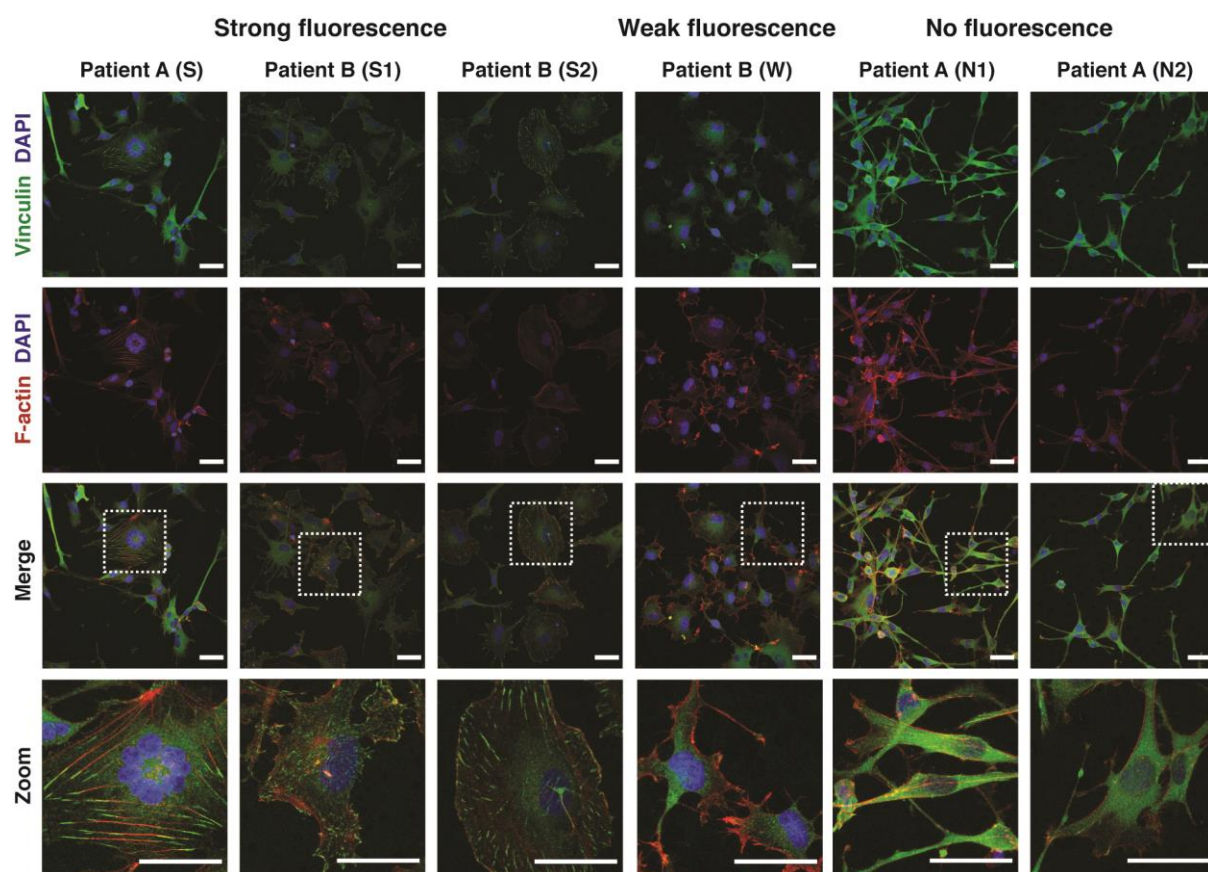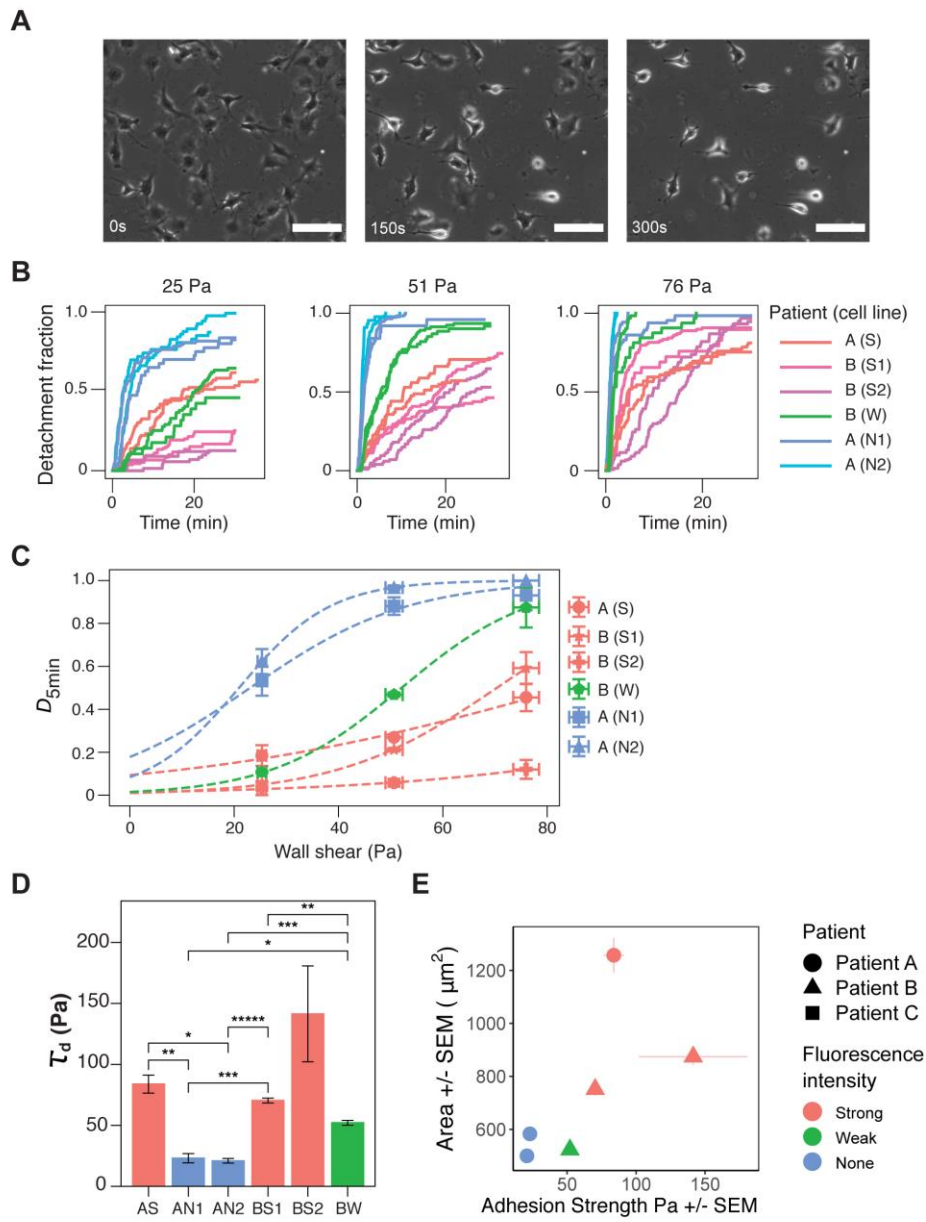
Figure 1

Figure 2

Figure 3

Figure 4

**A**



**B**

**C**